A comparative theoretical study on core-hole excitation spectra of azafullerene and its derivatives

Yunfeng Deng, Bin Gao, Mingsen Deng, and Yi Luo

Citation: The Journal of Chemical Physics **140**, 124304 (2014); doi: 10.1063/1.4868717
View online: http://dx.doi.org/10.1063/1.4868717
View Table of Contents: http://scitation.aip.org/content/aip/journal/jcp/140/12?ver=pdfcov
Published by the AIP Publishing

A comparative theoretical study on core-hole excitation spectra of azafullerene and its derivatives

Yunfeng Deng,[1,2] Bin Gao,[1,3,a)] Mingsen Deng,[1,b)] and Yi Luo[1,4]
[1]*Guizhou Provincial Key Laboratory of Computational Nano-material Science, Guizhou Normal College, Guiyang 550018, China*
[2]*Department of Physics, Guizhou University, Guiyang 550025, China*
[3]*Centre for Theoretical and Computational Chemistry (CTCC), Department of Chemistry, University of Tromsø—The Arctic University of Norway, N-9037 Tromsø, Norway*
[4]*Department of Theoretical Chemistry, School of Biotechnology, Royal Institute of Technology, SE-10691 Stockholm, Sweden*

(Received 1 January 2014; accepted 6 March 2014; published online 24 March 2014)

The core-hole excitation spectra—near-edge x-ray absorption spectroscopy (NEXAFS), x-ray emission spectroscopy (XES), and x-ray photoelectron spectroscopy (XPS) shake-up satellites have been simulated at the level of density functional theory for the azafullerene $C_{59}N$ and its derivatives $(C_{59}N)^+$, $C_{59}HN$, $(C_{59}N)_2$, and $C_{59}N–C_{60}$, in which the XPS shake-up satellites were simulated using our developed equivalent core hole Kohn-Sham (ECH-KS) density functional theory approach [B. Gao, Z. Wu, and Y. Luo, J. Chem. Phys. **128**, 234704 (2008)] which aims for the study of XPS shake-up satellites of large-scale molecules. Our calculated spectra are generally in good agreement with available experimental results that validates the use of the ECH-KS method in the present work. The nitrogen *K*-edge NEXAFS, XES, and XPS shake-up satellites spectra in general can be used as fingerprints to distinguish the azafullerene $C_{59}N$ and its different derivatives. Meanwhile, different carbon *K*-edge spectra could also provide detailed information of (local) electronic structures of different molecules. In particular, a peak (at around 284.5 eV) in the carbon *K*-edge NEXAFS spectrum of the heterodimer $C_{59}N–C_{60}$ is confirmed to be related to the electron transfer from the $C_{59}N$ part to the C_{60} part in this charge-transfer complex. © *2014 AIP Publishing LLC*. [http://dx.doi.org/10.1063/1.4868717]

I. INTRODUCTION

Heterofullerenes as one of the fullerene derivatives—in which one or more cage carbon atoms are replaced by other heteroatoms—have received particular attention since their discovery. They are believed to possess different electronic and chemical characteristics than pure carbon cages, and are anticipated to have applications, for instance, in superconducting materials and photodiode-based devices.[1,2]

Among different heterofullerenes, the aza[60]fullerene dimer $(C_{59}N)_2$ is probably the most known one and with macroscopic synthetic methods developed independently by the group of Wudl[3] and the group of Hirsch.[4] As such, $(C_{59}N)_2$ as well as its functional derivatives have been extensively examined by both theoreticians and experimentalists,[5] for instance, its electron energy loss spectroscopy (EELS),[6–8] vibrational and Raman spectra,[7,9] electron spin resonance (ESR),[10] nuclear magnetic resonance (NMR),[11] and x-ray absorption and x-ray photoelectron spectroscopy (XAS and XPS),[8,12–14] have all been investigated and used to reveal its stability, electronic, and chemical properties.

It is known from these studies, especially from the theoretical calculations and the XAS spectra at the carbon and nitrogen *K*-edge, that the highest occupied molecular orbital (HOMO) in the aza[60]fullerene dimer $(C_{59}N)_2$ is predominantly concentrated on the nitrogen atoms and the intermolecular bond, while the lowest unoccupied molecular orbital (LUMO) has strong carbon character.[7,8,13,15] This gives a very different picture from that of a single C_{60} or $C_{59}N$ molecule.[7,8]

The problem of the $C_{59}N$ monomer is its unpaired electron which makes itself a rather reactive radical,[15] such that it was until recently synthesized by doping into the crystalline C_{60},[16,17] in which the $C_{59}N$ molecules exist either in the form of heterodimers $C_{59}N–C_{60}$ or dissociated monomers.[17] It was further confirmed from the *ab initio* calculations that the electron spin density of the heterodimer $C_{59}N–C_{60}$ resides mostly on the C_{60} part.[17] Even though its instability, the studies of the $C_{59}N$ monomer is still an active field. For instance, by utilizing its half-occupied molecular orbital, Zhao *et al.* have proposed its use as the molecular rectifier.[18] The hyperfine couplings of the $C_{59}N$ monomer have also been studied at different theoretical levels.[19,20]

Another two simple but important members in the $C_{59}N$ family are the hydroazafullerene $C_{59}HN$ and the ion $(C_{59}N)^+$. The former has been studied much earlier as a simple saturated molecule from the parent radical, but which is also the parent for other hydroheterofullerenes.[21] The latter was until recently recognized as a key intermediate in the synthesis of other heterofullerenes.[5,22]

To briefly summarize here, the replacement of one or more cage carbon atoms has opened up a new and rich

a)bin.gao@uit.no
b)deng@gznc.edu.cn

field in fullerene science—"cage modification chemistry,"[1] in which the aza[60]fullerene and its functional derivatives have played an important role in this area.[5] Therefore, understanding their electronic and chemical properties is paramount for their further studies and applications. Many efforts have been devoted to obtaining such knowledge as addressed in the aforementioned studies, in which one may notice the role of different x-ray spectra as valuable experimental techniques to probe the electronic structures of the aza[60]fullerene dimer $(C_{59}N)_2$,[8,12–14] and even the monomer $C_{59}N$ on the silicon surface.[23]

The near-edge x-ray absorption spectroscopy (NEXAFS) is a well-known spectroscopic approach to detect the local structures of molecules, and the information of unoccupied molecular orbitals. As complementary, the x-ray emission spectroscopy (XES) is usually used to probe the occupied density of electronic states of molecules. Both NEXAFS and XES are element and site specific, which make them a powerful technique to determine detailed electronic properties of materials. The x-ray photoelectron spectroscopy (XPS) shake-up satellites as used in Refs. 12 and 14 result from the valence electron excitations accompanied with the core electron ionization, and it therefore could provide information of the valence band of materials under the screening of the core hole. Although there are many developed methods for the simulations of NEXAFS and XES spectra at a relatively high theoretical level, for instance, the full core-hole potential method for NEXAFS at the level of density functional theory (DFT),[24–26] the simulation of the XPS shake-up satellites of large-scale molecules still presents great challenge for computations at high theoretical level. Brena *et al.* have recently proposed an approach to calculate the shake-up satellites based on the equivalent core hole time-dependent density functional theory (ECH-TDDFT),[27,28] in which the core hole has been approximated by the equivalent core (also donated as $Z+1$ approximation), and the valence excitations in the presence of the core hole are computed by using TDDFT calculations within the $Z+1$ approximation. The applicability of the ECH-TDDFT approach has been demonstrated by simulations of the shake-up satellites of benzene and another rather large molecule—metal free phthalocyanine.[27,28]

Our recently developed equivalent core hole Kohn-Sham (ECH-KS) density functional theory approach[29] has enforced further approximations in the simulations of the XPS shake-up satellites, in which only the one-electron transition between molecular orbitals within core-hole potential is considered. Notice that the one-electron transition is often the dominant process for shake-up, the calculated shake-up satellites from the ECH-KS approach show remarkable agreement with results of the ECH-TDDFT calculations and available experiments.[29] The ECH-KS approach is therefore expected to provide reliable assignments for the complicated shake-up spectra of large-scale systems.

The purpose of the current work is therefore to provide a comparative theoretical study on the NEXAFS, XES, and XPS shake-up satellites of five representative members in the $C_{59}N$ family—$C_{59}N$, $(C_{59}N)^+$, $C_{59}HN$, $(C_{59}N)_2$, and $C_{59}N$–C_{60} based on the full core-hole potential method and our developed ECH-KS approach, respectively. Although the NEXAFS and XPS shake-up satellites of the aza[60]fullerene dimer $(C_{59}N)_2$ and the NEXAFS spectrum of the monomer $C_{59}N$ (on the silicon surface) have been reported,[8,12–14,23] we are unaware of such a study on other $C_{59}N$ family members, especially a detailed theoretical study. As such, our current study could provide valuable results to assist further experimental measurements on these heterofullerenes and derivatives.

The paper is organized as follows: the computational details are given in Sec. II, while the results and discussion are presented in Sec. III, including the electronic structures, NEXAFS, XES, and XPS shake-up satellites of the five $C_{59}N$ family members—$C_{59}N$, $(C_{59}N)^+$, $C_{59}HN$, $(C_{59}N)_2$, and $C_{59}N$–C_{60}. And our final conclusions are given in Sec. IV.

II. COMPUTATIONAL DETAILS

As shown in Fig. 1(a), we have plotted the nitrogen atom and its three connected carbon atoms in the $C_{59}N$ monomer, in which the atoms C_2 and C_2' are symmetric equivalent. As revealed from previous studies for instance Ref. 15, the link between the $C_{59}N$ monomer and hydrogen, another $C_{59}N$ moiety or C_{60} is made by a specific nearest neighbour of the nitrogen atom, which is the atom C_1 in Fig. 1(a). All the geometries of $C_{59}N$, $(C_{59}N)^+$, $C_{59}HN$, $(C_{59}N)_2$, and $C_{59}N$–C_{60} were optimized at B3LYP/6-31G(d) level using Gaussian 09 program[30] in the current work and were confirmed to be the minimum energy structure by frequency calculations. These optimized structures were then used in the calculations of core-hole excitation spectra.

Within the dipole approximation and sudden approximation,[31,32] the intensities of the NEXAFS and XES spectra are mostly governed by the dipole transition moments $\langle\psi_i|\boldsymbol{r}|\psi_f\rangle$ $(\boldsymbol{r}=x,y,z)$, where ψ_i and ψ_f are, respectively, the molecular orbitals (MOs) of the initial and final states $|i\rangle$ and $|f\rangle$. In practice, the final state rule is often used to simplify the calculations of the NEXAFS and XES spectra. This rule was first developed by von Barth and Grossman[33] in 1979 for the calculation of the XES spectra of simple metals, and was later generalized to the NEXAFS and XES spectra of finite molecular systems by Privalov, Gel'mukhanov, and Ågren.[34,35] According to the final state rule, the accurate NEXAFS and XES spectra could be obtained by only considering the final state wave functions of the processes, i.e., valence hole states for the XES, and core excited states for the NEXAFS.

Although the final state rule has greatly simplified the computational procedure for the NEXAFS spectra, it is still not feasible to get the transitions to all possible final states from a state-by-state approach. The situation becomes even worse for large systems with lots of MOs, especially a large number of virtual MOs, which makes it impracticable to access all the possible final states. A solution is to find one reference electronic configuration which could represent the characters of all transitions, so that the spectrum in a wide energy range can be generated from a single calculation.[32] Various approximations have been proposed to mimic the reference

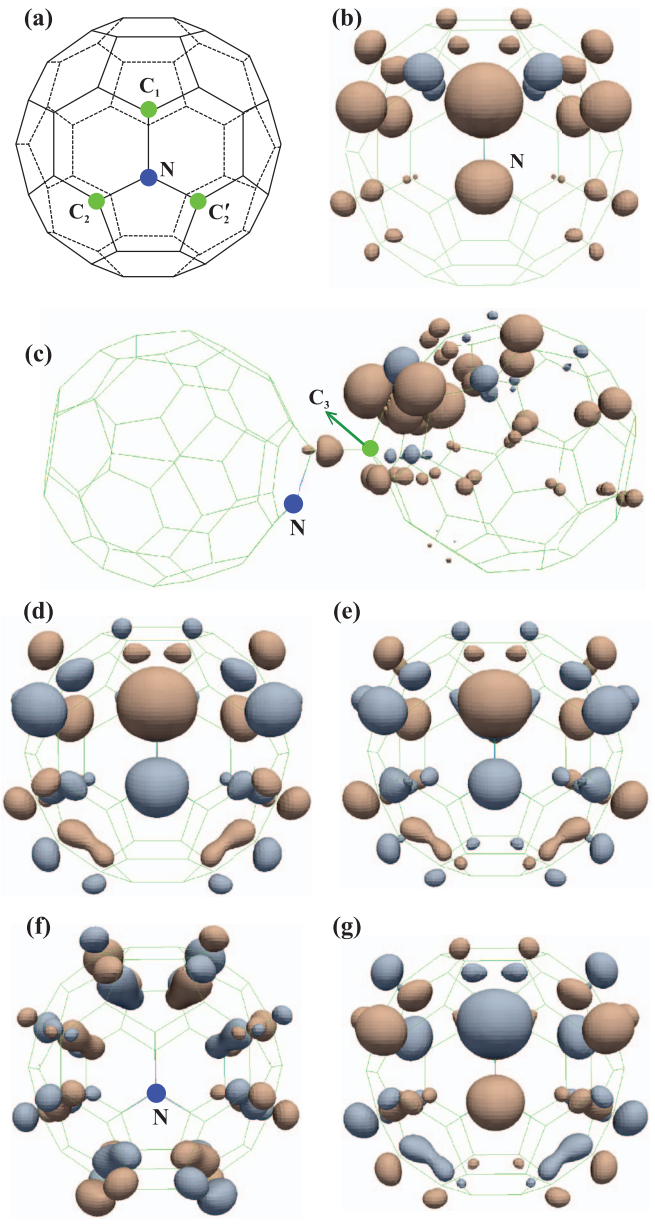

FIG. 1. (a) Molecular structure of $C_{59}N$ monomer and carbon atoms connected to the nitrogen atom, in which the atoms C_2 and C_2' are symmetric equivalent; (b) and (c) Electron spin density of the $C_{59}N$ monomer and $C_{59}N$–C_{60} molecule calculated at B3LYP/6-311+G* level; (d) and (e) The HOMO (α-spin) and LUMO (β-spin) of the $C_{59}N$ molecule calculated at B3LYP/6-311+G* level; (f) and (g) The HOMO and LUMO of $(C_{59}N)^+$ ion calculated at B3LYP/6-311+G* level.

electronic configuration, such as the $Z+1$ approximation and transition potential method.[36]

As regarding fullerenes, azafullerenes, and their derivatives, many studies have confirmed the necessity of using the so-called full core-hole (FCH) potential method for a reliable description of their NEXFAS spectra.[24–26,37,38] In this method, the reference electronic configuration is chosen as a core-ionized state by neglecting the core-excited electron which is believed to have smaller influence than the core hole, and special basis set is usually recommended for the excited atom.[32] In the current study, we choose the triple-ζ quality individual gauge for localized orbital (IGLO-III) basis set of Kutzelnigg, Fleischer, and Shindler[39] for the excited carbon or nitrogen atom, while other non-excited atoms are described by model core potentials to facilitate the convergence of the core-hole state. An even larger basis set—an augmented diffuse basis set (19*s*, 19*p*, 19*d*) is then used for the excited carbon or nitrogen atom in the NEXAFS spectra calculations.

To further get the absolute energy position of the NEXAFS spectra, the ΔKohn-Sham (ΔKS) method has to be employed.[24] As such, all the calculated NEXAFS spectra are calibrated so that the first spectral feature corresponding to the transition from the 1*s* level to the LUMO coincides with the same one obtained from the ΔKS calculations in which the energy difference between the ground state and the relaxed core-excited state is calculated. The ionization potentials (IPs) are also calculated in the ΔKS scheme where the energy is taken as the difference between the ground state and the fully optimized core-ionized state.

In the present study, all the NEXAFS spectra calculations and the ΔKS calculations were performed with the gradient-corrected Becke (BE88) exchange functional[40] and the Perdew (PD86) correlation functional[41] by using StoBe-deMon software.[42] The relativistic effects of +0.2 eV for the carbon *K*-edge and +0.3 eV for the nitrogen *K*-edge[43] were also included to produce the overall shift of the calculated spectra. The NEXAFS spectra were finally generated by a Lorentzian convolution of the discrete intensities with varying broadening. For the region below the IP the full width at half maximum (FWHM) was set to 0.3 eV, for the next 5 eV the FWHM is linearly increased up to 1.0 eV and at higher energies a constant FWHM of 1.0 eV was applied.

In the case of XES spectra, the evaluation of the valence hole states is needed according to the final state rule.[33–35] This could be simplified further by neglecting the effect of the valence hole, and evaluating the XES intensity[32]

$$I^{\mathrm{XES}}(\varepsilon_{if}) \propto \varepsilon_{if}^3(|\langle\psi_i|x|\psi_f\rangle|^2+|\langle\psi_i|y|\psi_f\rangle|^2+|\langle\psi_i|z|\psi_f\rangle|^2), \tag{1}$$

by using the wave functions from a ground state electronic structure calculation. Here, $\epsilon_{if} = \epsilon_i - \epsilon_f$ is the MO energy difference, and ψ_i and ψ_f are, respectively, the valence and core orbitals of the ground state. The neglect of the valence hole in the XES spectra calculations has been well tested in many studies, see for instance, Refs. 26, 32, and 37 and references therein.

The XES spectra were simulated using our developed tool package BioNano-LEGO Version 2.0[44] after obtaining the wave functions of the ground state from Gaussian 09 program.[30] All the possible transition moments involved in Eq. (1) were calculated at B3LYP/6-311+G* level. The computed XES spectra were also convoluted by a Lorentzian function with FWHM as 0.3 eV.

Based on the work of Martin,[45] the intensity ratio of the *n*th XPS shake-up peak to the main peak can be written as

$$\frac{I(n)}{I(0)} \simeq \frac{\left|\sum_{n'} a_{nn'} S_{n'}\right|^2}{\left|\sum_{n'} a_{0n'} S_{n'}\right|^2}, \tag{2}$$

where $a_{nn'}$ and $a_{0n'}$ are the configuration interaction expansion coefficients, and $S_{n'}$ is the overlap between the excited "configuration state function" (CSF) $\psi_f^{(n')}$ and the wave function of the ground state ψ_g

$$S_{n'} = \langle \psi_f^{(n')} | \psi_g \rangle. \quad (3)$$

Therefore, in contrast to the NEXAFS and XES spectra, the dominant factor that governs the intensity of the XPS shake-up satellites is not the dipole transition moment, but the overlap, or the so-called monopole transition $S_{n'}$.[46,47]

The key approximation made in the ECH-TDDFT method is the replacement of the core hole by the equivalent core, and that the valence electron excitations are calculated from the TDDFT calculations in the presence of the equivalent core.[27,28] The use of the ECH approximation in the XPS shake-up satellites has already been illustrated in several semiempirical computations.[48–50] The combination of the ECH approximation and the TDDFT technique provides an efficient and accurate procedure for the computations of all possible multiple valence electron excitations with inclusion of the electron correlation.[27,28] The applicability of the ECH-TDDFT approach has been demonstrated by Brena *et al.* in the studies of the XPS shake-up satellites of benzene, metal free phthalocyanine, and nickel phthalocyanines.[27,28,51]

The limitation of the ECH-TDDFT approach resides in the TDDFT calculations at the current level of computational capacities, especially in the case of large-scale molecules—in which it is still not feasible for the present TDDFT calculations to compute the numerous excited states for the XPS shake-up satellites. In the recent study by Gao *et al.*,[29] the ECH-KS method has been proposed for the computations of the XPS shake-up satellites, which enforces further approximation in comparison to the ECH-TDDFT approach—using the molecular orbital to represent the molecular state in a one-electron sudden approximation. Apparently, the configuration interaction is neglected in the ECH-KS method, so that some details in the XPS shake satellites will be lost. However, as demonstrated in Ref. 29, the results from the ECH-KS approach show remarkable agreement with those from the ECH-TDDFT calculations and available experiments, such as different fullerenes and carbon nanotubes.[29] The encouraging performance of the ECH-KS approach could be understood from the fact that the dominated excitation in the XPS shake-up processes is often from one particular excitation channel. Therefore, neglecting the configuration interaction will not affect the assignments of the main spectral features in the XPS shake-up satellites.[29]

Moreover, for systems that the first excited state could be got from the ECH-TDDFT approach, one can further calibrate the ECH-KS results by lining up its first state to that of the ECH-TDDFT calculations. Therefore, we have chosen the ECH-KS approach in our current study for the computations of the XPS shake-up satellites. The calculations were carried out at B3LYP level using the tool package BioNano-LEGO Version 2.0.[44] The 6-31G basis set was used for the non-ionized atoms, while the IGLO-III basis set of Kutzelnigg, Fleischer, and Shindler[39] was employed for the core-ionized carbon or nitrogen atom (or the substituted nitrogen or oxygen atom in the ECH approximation). The positions of main lines (IPs) were obtained from the ΔKS approach during the procedure of the NEXAFS spectra simulations. The calculated discrete shake-up intensities were further calibrated using the ECH-TDDFT calculations as aforementioned, i.e., the first spectral feature corresponding to the transition to the first electronic excited state was lined up to that from the ECH-TDDFT calculations. Afterwards, the shake-up intensities were convoluted with a Lorentzian function of 0.3 eV FWHM to obtain the final XPS shake-up spectra.

III. RESULTS AND DISCUSSION

Before presenting the results of different core-hole excitation spectra of the $C_{59}N$ family members, it could be interesting and necessary to discuss their electronic structures from our calculations. First, we have the binding energies (BE) of hydrogen atom, $C_{59}N$ and C_{60} to the $C_{59}N$ monomer from

$$E_{BE} = E_{C_{59}N-X} - (E_{C_{59}N} + E_X), \quad (4)$$

where $E_{C_{59}N-X}$ is the electronic energy of molecules $C_{59}HN$, $(C_{59}N)_2$ or $C_{59}N$–C_{60}, $E_{C_{59}N}$ is the electronic energy of the isolated $C_{59}N$ monomer, and E_X the electronic energy of the isolated hydrogen atom, $C_{59}N$ or C_{60} molecule. The calculated binding energies at B3LYP/6-311+G* level are −77.519 ($C_{59}HN$), −31.155 (($C_{59}N)_2$), and −0.390 ($C_{59}N$–C_{60}) kcal/mol. It is clear that the $C_{59}N$–C_{60} molecule is quite a weakly bonded dimer when comparing with the other two.

However, an interesting phenomenon of the $C_{59}N$–C_{60} molecule is the distribution of its electron spin density, which does not reside on the $C_{59}N$ part but on the C_{60} part.[17] In Figs. 1(b) and 1(c), we have plotted, respectively, the electron spin densities of the $C_{59}N$ monomer and the $C_{59}N$–C_{60} molecule from calculations at B3LYP/6-311+G* level. These densities are visualized using ParaView program[52] with an isovalue as 0.004. From which, one can clearly observe the transfer of electron spin density from the $C_{59}N$ monomer to the C_{60} part, with a few left on the link carbon atom C_1.

In Fig. 2, we further plot the binding energies between the $C_{59}N$ and C_{60} parts, and Mulliken atomic spin densities of these two parts as a function of the bond length of the $C_{59}N$–C_{60} heterodimer. From which, we can conclude that the energy difference between the heterodimer $C_{59}N$–C_{60} and dissociated pair of the $C_{59}N$ and C_{60} molecules is small, with a barrier 8.69 kcal/mol as the bond length around 2.1 Å, which is close to ∼11.53 kcal/mol as reported by Rockenbauer *et al.*[17] From the Mulliken atomic spin densities in Fig. 2, one can find around one electron transfer from the $C_{59}N$ part to the C_{60} part at its energy minimum structure with the bond length between these two parts as 1.600 Å. However, during the dissociation of the heterodimer, the electron is transferred back from the C_{60} part to the $C_{59}N$, in which the spin density is almost equally distributed on these two parts at the binding energy barrier ∼2.1 Å.

In their studies of the heterodimer $C_{59}N$–C_{60}, Rockenbauer *et al.* also found there was no more heterodimer detected above 360 K in the experiment, and the experimental

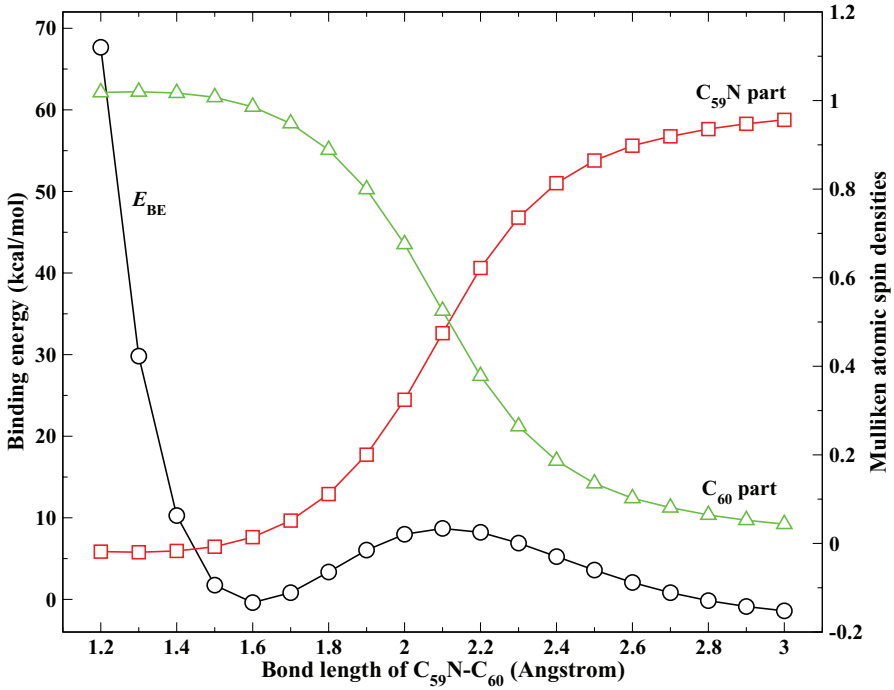

FIG. 2. Binding energies (black circles) between the $C_{59}N$ and C_{60} parts, and Mulliken atomic spin densities of these two parts ($C_{59}N$: red squares, C_{60}: green triangles) as a function of the bond length of the $C_{59}N$–C_{60} molecule.

configuration fluctuates between the heterodimer and dissociated molecules at finite temperatures.[17] Based on these theoretical and experimental results, we can conclude that the $C_{59}N$–C_{60} is indeed a charge-transfer complex, or a donor–acceptor non-covalent compound,[53] which is usually subject to temperature, and has small binding energy in the comparison to the covalently bonded molecules, such as the $C_{59}HN$ and $(C_{59}N)_2$ molecules.

One may therefore expect such difference in the electronic structures of the $C_{59}N$ family members could be revealed from the spectroscopic techniques, as which will be discussed in Secs. III A–III C.

A. Carbon *K*-edge NEXAFS and XES

In the left panel of Fig. 3, we give the calculated NEXAFS spectra at the carbon *K*-edge of molecules $C_{59}N$, $(C_{59}N)^+$, $C_{59}HN$, $(C_{59}N)_2$, and $C_{59}N$–C_{60}. The MO transitions from the carbon 1*s* orbital to the LUMO, LUMO+1, and LUMO+2 are also shown as red, green, and blue bars under the NEXAFS spectrum of each molecule, in which the contributions from the β-spin electrons are given as negative numbers in the $C_{59}N$ and $C_{59}N$–C_{60} molecules. For comparison, the NEXAFS spectrum of the C_{60} molecule (I_h symmetry) is also given at the bottom of this panel together with its discrete intensities as red bars. Obviously, both the five $C_{59}N$ family members and the C_{60} molecule possess four different peaks (features) A–D at almost the same energy positions in their NEXAFS spectra. However, one can still observe a few distinct differences among them. For instance, comparing with the C_{60} molecule, there are more MO transitions from the carbon 1*s* orbital to the unoccupied orbitals in each peak of the NEXAFS spectra of the five $C_{59}N$ family members due to their lower symmetry—C_{2h} for $(C_{59}N)_2$, and C_s for other four members.

Generally, the NEXAFS spectrum of the $(C_{59}N)^+$ ion resemble that of the $C_{59}N$—both have a relatively weak and broad peak B and a strong peak C. While the spectra of other three molecules $C_{59}HN$, $(C_{59}N)_2$, and $C_{59}N$–C_{60} fall into another category, in which the peak B becomes a bit stronger than the peak C, and a very weak feature A′ between the peaks A and B can be observed. This feature A′ as revealed by the MO transitions in Fig. 3 is mainly due to the carbon 1*s* orbital to the LUMO+2. The transition $1s \rightarrow \text{LUMO} + 2$ however either locates at higher energies close to the peak B in $C_{59}N$, or is much weaker and locates at lower energies close to the peak A in $(C_{59}N)^+$. Therefore, the feature A′ is directly related to the change of electronic structures of the $C_{59}N$ molecule after removing one electron or connecting with another atom or molecule.

We have also plotted individual contributions from the C_{60} and $C_{59}N$ parts of the $C_{59}N$–C_{60} molecule to its NEXAFS spectrum, as the red and green dashed lines under the spectrum of the $C_{59}N$–C_{60} in Fig. 3. One can immediately observe similar profiles of these two individual contributions, which in other words do not show the same profile as those of the single C_{60} (I_h symmetry) and $C_{59}N$ molecules. Therefore, even the $C_{59}N$–C_{60} is a weakly bonded molecule, its electronic structure does change in such a way that could be revealed from the spectra. For instance, as shown in Fig. 4, the arising feature A′ in the spectrum of the C_{60} part (bottom) and the blue-shifted peak B in the $C_{59}N$ part (top) comparing, respectively, with the single C_{60} and $C_{59}N$ molecules. It is worth pointing out that the peak A in the single C_{60} (I_h) molecule arises from the transition of the carbon 1*s* orbital to the LUMO, in which the LUMO, LUMO+1, and LUMO+2 are threefold

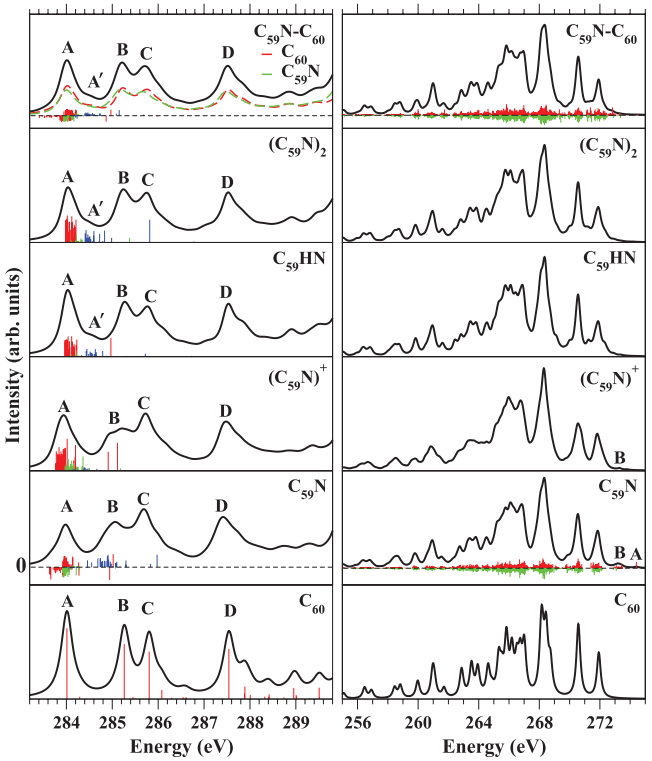

FIG. 3. Simulated NEXAFS (left) and XES (right) spectra at the carbon *K*-edge of the $C_{59}N$ family members and the C_{60} molecule. The transitions from the 1*s* to the LUMO (red bars), LUMO+1 (green bars), and LUMO+2 (blue bars) in the NEXAFS spectra of the $C_{59}N$ family members, and the discrete intensities (red bars) of the NEXAFS spectrum of the C_{60} molecule are also plotted under each convoluted spectrum, in which contributions from the β-spin electrons are given as negative numbers in the $C_{59}N$ and $C_{59}N$–C_{60} molecules. The individual contributions from the C_{60} and $C_{59}N$ parts of the $C_{59}N$–C_{60} molecule to the NEXAFS spectrum are also given as red and green dashed lines under the total spectrum. The discrete XES intensities of the $C_{59}N$ and $C_{59}N$–C_{60} are presented as red (α-spin) and green (β-spin, shown as the negative numbers) bars under the convoluted XES spectra.

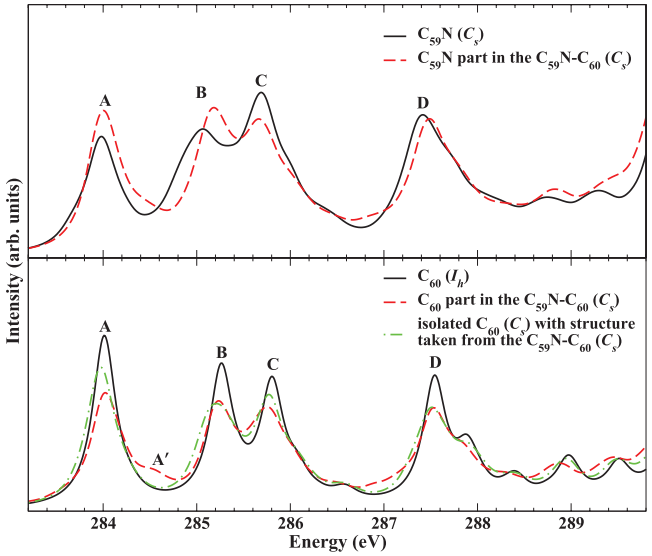

FIG. 4. Top: the NEXAFS spectrum at the carbon *K*-edge of the $C_{59}N$ molecule (solid) and the individual contribution from the $C_{59}N$ part to the NEXAFS spectrum of the $C_{59}N$–C_{60} molecule (dashed). Bottom: the NEXAFS spectrum of the C_{60} molecule (solid), the individual contribution from the C_{60} part of the $C_{59}N$–C_{60} molecule (dashed), and the NEXAFS spectrum of a single C_{60} molecule with geometric structure taken from the $C_{59}N$–C_{60} molecule (dotted-dashed).

degenerate with t_{1u} symmetry from ground state calculation. Such degeneration is removed in the $C_{59}N$–C_{60} molecule due to its lower symmetry C_s. But does the loss of degeneration or lower symmetry account for the arising of the feature A′ in the C_{60} part of the $C_{59}N$–C_{60} molecule? By noticing that there is no such feature A′ in the spectrum of the $C_{59}N$ part of the $C_{59}N$–C_{60} molecule, and the appearances of A′ in the spectra of the $C_{59}HN$ and $(C_{59}N)_2$ molecules, we could speculate that the feature A′ in the $C_{59}N$–C_{60} molecule should be related to the electron transfer from the $C_{59}N$ part to the C_{60} part.

This speculation can be further confirmed by checking the NEXAFS spectrum of the C_{60} part without electron transfer. As shown at the bottom of Fig. 4, we present the NEXAFS spectrum of the single C_{60} (I_h) molecule (solid), the contribution from the C_{60} part of the $C_{59}N$–C_{60} molecule to its NEXAFS spectrum (dashed), and the NEXAFS spectrum of a single C_{60} molecule with geometric structure taken from the $C_{59}N$–C_{60} molecule (dotted-dashed). Apparently, only the spectrum of the C_{60} part with electron transferred from the $C_{59}N$ moiety possesses the feature A′, while other two do not produce such a feature.

We have further analyzed the contributions of symmetric inequivalent atoms to the NEXAFS spectrum of each $C_{59}N$ family member. However, almost all the carbon atoms show similar NEXAFS spectral features A, B, C, and D, regardless different $C_{59}N$ family members. One exception is the feature A, which does not have the contributions from the three nearest carbon neighbours of the nitrogen atom, C_1, C_2, and C_2' as shown in Fig. 1(a). The difference of the feature A between the spectra of the neighbours of the nitrogen and other carbons can be well understood from their different local (chemical) environment.

Next, we turn our focus to the XES spectra at the carbon *K*-edge of these five $C_{59}N$ family members in the right panel of Fig. 3, in which we also give the XES spectrum of the C_{60} molecule at the bottom for comparison. The discrete XES intensities of the $C_{59}N$ and $C_{59}N$–C_{60} molecules are also shown as red (α-spin) and green (β-spin, shown as the negative numbers) bars under their convoluted XES spectra.

Unlike the NEXAFS spectra, except for the peaks A (dominated by the MO transition from the HOMO (α spin) to the 1*s* orbital of the carbon atom C_1) and B (transitions from the HOMO to the 1*s* orbitals of other carbon atoms) in the $C_{59}N$ molecule and the peak B in the $(C_{59}N)^+$, we cannot see other visible differences in the XES spectra of these five $C_{59}N$ family members, and they also show quite similar XES spectra to that of the C_{60} molecule. Therefore, although it may not be trivial from the experimental aspect, the feature A′ in the NEXAFS spectrum of the $C_{59}N$–C_{60} molecule and the peaks A and B in the XES spectrum of the $C_{59}N$ could be used together to examine their existences in the C_{60} crystalline.[17]

B. Nitrogen *K*-edge NEXAFS and XES

As regards another important family member $(C_{59}N)^+$ ion, it may be hard to detect its existence from the aforementioned carbon *K*-edge NEXAFS and XES spectra. However,

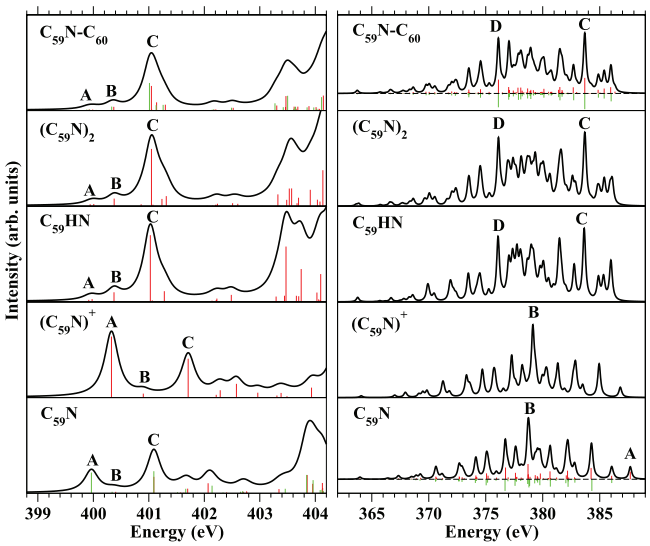

FIG. 5. Left: simulated NEXAFS spectra (with discrete intensities before convolution as red (α-spin) and green (β-spin) bars) at the nitrogen K-edge of $C_{59}N$, $(C_{59}N)^+$, $C_{59}HN$, $(C_{59}N)_2$, and $C_{59}N$–C_{60} molecules. Right: calculated XES spectra at the nitrogen K-edge of these five molecules, in which the discrete XES intensities of the $C_{59}N$ and $C_{59}N$–C_{60} molecules are also shown as red (α-spin) and green (β-spin, shown as the negative numbers) bars under their convoluted XES spectra.

as shown in the left panel of Fig. 5, the NEXAFS spectrum at the nitrogen K-edge could be employed to examine its existence from the very strong peak A, which comes from the transition of nitrogen 1s to the LUMO. On the contrary, the nitrogen 1s → LUMO transition only results in a weak shoulder A at lower excitation energies in the molecules $C_{59}HN$, $(C_{59}N)_2$ and $C_{59}N$–C_{60}. In the case of the $C_{59}N$ molecule, the β-spin nitrogen 1s → LUMO transition also produces the first peak A with moderate intensity at lower excitation energy. Although the core-hole effect is important for the understanding of NEXAFS spectra, such a difference in the nitrogen 1s → LUMO transition in these five molecules could still be understood from the distribution of their LUMOs in the ground state. We present the LUMOs of the molecules $C_{59}N$ (β-spin) and $(C_{59}N)^+$ in Figs. 1(e) and 1(g), which were calculated at B3LYP/6-311+G* level in the ground state. Unlike the $(C_{59}N)_2$ molecule whose LUMO has strong carbon character,[7,8,13,15] the LUMOs of the $C_{59}N$ and $(C_{59}N)^+$ molecules given here also have obvious distribution around the nitrogen atom. As such, a strong or moderate peak A could be observed in their NEXAFS spectra. Especially, the quite strong peak A and its relatively high excitation energy in the $(C_{59}N)^+$ ion could be used as the fingerprint of its existence.

By using the information from the ground state calculations, we could also understand the XES spectra at the nitrogen K-edge. As shown in the right panel of Fig. 5, we can see a clear peak A at high energy in the XES spectrum of the $C_{59}N$ molecule, which arises from the transition of the HOMO (α-spin) to the nitrogen 1s orbital. As shown in Fig. 1(d), the HOMO (α-spin) of the $C_{59}N$ molecule has a strong nitrogen character, which therefore produces an observable peak A in its XES spectrum. However, in the case of the $(C_{59}N)^+$ ion, its HOMO as shown in Fig. 1(f) has strong carbon character, so that the transition from the HOMO to the nitrogen 1s does not result in any observable peak in its XES spectrum. As regards other three molecules, $C_{59}HN$, $(C_{59}N)_2$, and $C_{59}N$–C_{60}, although their HOMOs also have some nitrogen character, the transition HOMO → nitrogen 1s happens at relatively lower energies comparing with that of the $C_{59}N$ molecule. Other noticeable features in the XES spectra include the sharp and strong peak B in the $C_{59}N$ and $(C_{59}N)^+$ molecules, the same

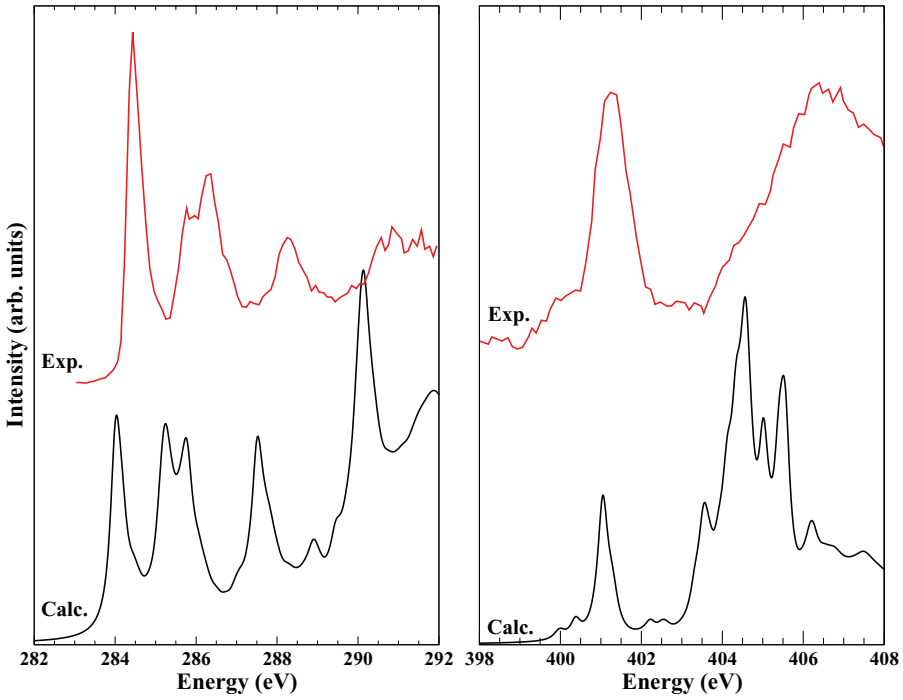

FIG. 6. Simulated NEXAFS spectra of $(C_{59}N)_2$ molecule at the carbon (left) and nitrogen (right) K-edge together with the experimental counterpart taken from Ref. 13.

strong and sharp peaks C and D in the molecules $C_{59}HN$, $(C_{59}N)_2$, and $C_{59}N$–C_{60}. These peaks are due to the transitions from deeper valence orbitals to the nitrogen 1*s* orbital(s), and may be used to distinguish different $C_{59}N$ family members.

Last but not least, we have compared our calculated NEXAFS spectra of the $(C_{59}N)_2$ molecule with those from the experiments.[13] As shown in Fig. 6, the results from our calculations are in general good agreement with the experimental counterparts both at the carbon *K*-edge and nitrogen *K*-edge. One may notice that the calculated NEXAFS spectra are red-shifted comparing with the corresponding experimental data, as well as the inconsistent relative intensities between the second and the third peaks at the carbon *K*-edge. These could be attributed to the choice of DFT functionals used in our calculations.[54] It, therefore, expects that the hybrid functional may improve the FCH potential method for the simulations of NEXAFS spectra, which is however out of the scope of the current work.

C. XPS shake-up satellites

The simulated XPS shake-up satellites at the carbon *K*-edge of molecules $C_{59}N$, $(C_{59}N)^+$, $C_{59}HN$, $(C_{59}N)_2$, and $C_{59}N$–C_{60} are given in Fig. 7, together with those of the C_{60} molecule at the bottom (with the discrete intensities as red bars). It should be noted that the XPS shake-up satellites of the $(C_{59}N)^+$ ion have been shifted −3.15 eV so that its observable XPS main line after convolution locates at the same energy position as that of the $C_{59}HN$ molecule. The XPS main lines of all symmetric inequivalent carbon atoms are shown as red bars under each spectrum of the $C_{59}N$ family members, in which the contributions from β-spin electrons are plotted as negative numbers and green bars in the $C_{59}N$ and $C_{59}N$–C_{60} molecules.

It is clear that the XPS shake-up satellites of the $C_{59}N$ family members display quite different profiles comparing with those of the C_{60} molecule, indicating the change of electronic structures (or more exactly the valence orbitals) after replacing one carbon atom with the nitrogen atom. We also notice that even the individual contributions from the C_{60} part of the $C_{59}N$–C_{60} molecule—denoted as the red dashed line at the top panel—are different from the XPS shake-up satellites of a single C_{60} molecule, which again confirms the change of valence orbitals of the C_{60} moiety in the $C_{59}N$–C_{60} molecule.

Among the XPS shake-up satellites of these five $C_{59}N$ family members, except for the energy shift of the $(C_{59}N)^+$ ion, others show quite similar profiles with noticeable peaks A and B close to the XPS main line. In Table I, we have assigned the dominant contributions to the peaks A and B in these five molecules. It is interesting that except for the peak B in the $C_{59}N$ and $(C_{59}N)^+$ molecules which are due to the shake-up processes, the dominant contributions to the peaks A and B in these five molecules are indeed the XPS main lines of the atoms C_1, C_2, and C_3. From Figs. 1(a) and 1(c), it is clear that the atom C_2 (sp^2-like) is connected to the nitrogen atom, while the atoms C_1 (connected to the nitrogen atom) and C_3 (in the $C_{59}N$–C_{60}) are more sp^3-like carbons in the molecules $C_{59}HN$, $(C_{59}N)_2$, and $C_{59}N$–C_{60}. As such, it is not surprising that their binding energies are a bit higher than those of other carbon atoms. We notice however that the binding energy of the C_1 atom (sp^2-like) in the $C_{59}N$ molecule is still close to the XPS main line, while it changes to a bit higher

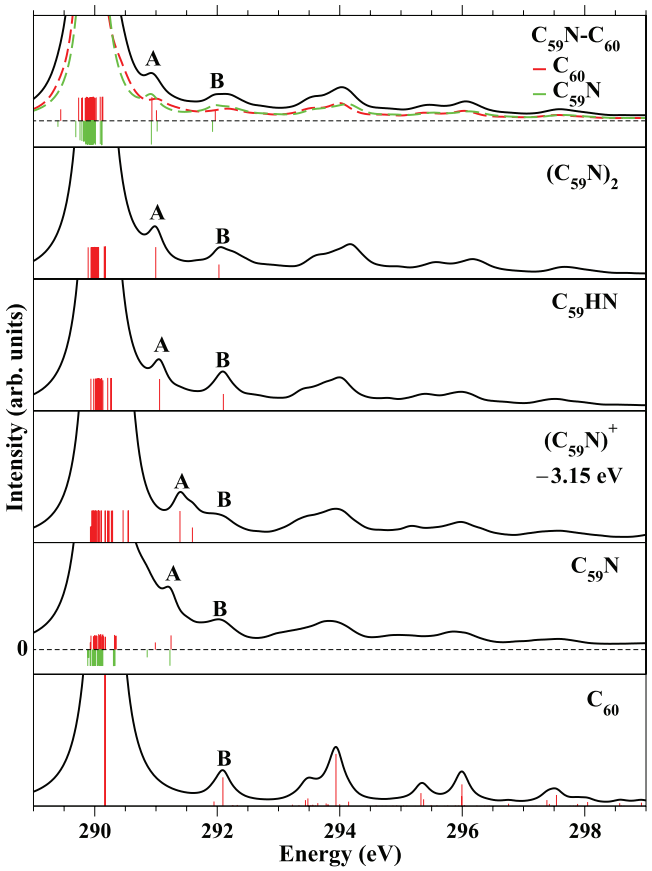

FIG. 7. Simulated XPS shake-up satellites at the carbon *K*-edge of $C_{59}N$, $(C_{59}N)^+$, $C_{59}HN$, $(C_{59}N)_2$, and $C_{59}N$–C_{60} molecules, together with those of C_{60} molecule at the bottom (discrete intensities before convolution are given as red bars). The XPS main lines of all symmetric inequivalent carbon atoms are also shown as red bars under each XPS shake-up spectrum of the $C_{59}N$ family members, in which contributions from the β-spin electrons are plotted as green bars in the $C_{59}N$ and $C_{59}N$–C_{60} molecules. The individual contributions from the C_{60} and $C_{59}N$ parts of the $C_{59}N$–C_{60} molecule to the XPS shake-up satellites spectrum are also given as red and green dashed lines under the total spectrum.

TABLE I. Assignments of the carbon *K*-edge XPS shake-up satellites of the $C_{59}N$ family members.

	A	B
$C_{59}N$	C_2: 291.245 eV (α)	...[a]
	C_2: 291.228 eV (β)	
$(C_{59}N)^+$	C_1: 294.744 eV	...[a]
	C_2: 294.542 eV	
$C_{59}HN$	C_2: 291.058 eV	C_1: 292.100 eV
$(C_{59}N)_2$	C_2: 291.000 eV	C_1: 292.028 eV
$C_{59}N$–C_{60}	C_2: 290.933 eV (α)	C_1: 291.968 eV (α)
	C_2: 290.925 eV (β)	C_1: 291.923 eV (β)
	C_3: 291.007 eV (α)	
	C_3: 291.019 eV (β)	

[a]XPS shake-up satellites contributed from several carbon atoms.

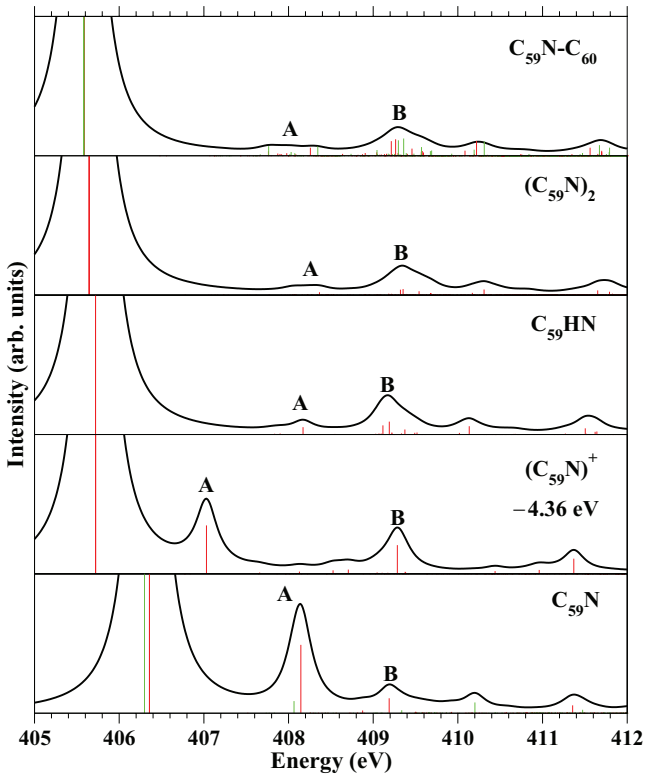

FIG. 8. Simulated XPS shake-up satellites at the nitrogen *K*-edge and the discrete intensities before convolution (red bars) of $C_{59}N$, $(C_{59}N)^+$, $C_{59}HN$, $(C_{59}N)_2$, and $C_{59}N$–C_{60} molecules. The contributions from the β-spin electrons in the $C_{59}N$ and $C_{59}N$–C_{60} molecules are also shown as green bars under the spectra.

value 294.744 eV in the $(C_{59}N)^+$ ion, but which is still sp^2-like and contributes to the peak A.

To briefly summarize, the replacement of one carbon atom with the nitrogen atom results in at least two sp^2-like carbons C_1 and C_2 with different local electronic structures comparing with other carbons. The binding energy of the atom C_2 is blue-shifted around 1 eV to the XPS main line, while that of the atom C_1 does not change in the $C_{59}N$ molecule. However, after removing one electron ($(C_{59}N)^+$ ion), or connected to other atoms (like hydrogen) or large molecules (such as $C_{59}N$ and C_{60}), the local electronic structures of the C_1 atom changes a lot (it becomes an sp^3-like carbon in the $C_{59}HN$, $(C_{59}N)_2$, and $C_{59}N$–C_{60} molecules) and that therefore results in a large blue-shifted binding energy—around 1.5 eV in the $(C_{59}N)^+$ ion and ~2 eV in other three molecules comparing with their XPS main line.

The changes of electronic structures can also be revealed from the nitrogen *K*-edge XPS shake-up satellites. As shown in Fig. 8, the XPS main line has gained a large blue-shifted after the $C_{59}N$ loses one electron becoming the $(C_{59}N)^+$ ion. Moreover, the peak A is more close to the main line in the $(C_{59}N)^+$ molecule. In the case of other three molecules $C_{59}HN$, $(C_{59}N)_2$, and $C_{59}N$–C_{60}, the distinctive difference is their quite weak peak A comparing with the $C_{59}N$ molecule. Therefore, the nitrogen *K*-edge XPS shake-up satellites provide a useful technique to detect the existence of the $C_{59}N$ and $(C_{59}N)^+$ molecules, which can also be used to distinguish them from other $C_{59}N$ family members.

In Table II, we have also assigned the main contributions to the peaks A and B in the nitrogen *K*-edge XPS shake-up satellites of these five $C_{59}N$ family members, which could be useful for further experimental studies. It is obvious that except for the $C_{59}N$ and $C_{59}HN$, the peak B also involves excitations from deeper valence orbitals in other three molecules.

Finally, we present in Fig. 9 our calculated XPS shake-up satellites of the $(C_{59}N)_2$ molecule and the experimental data[14] at the carbon *K*-edge, in which the calculated spectrum has been shifted by lining up its observable main line to that of the experimental data at 0 eV. It is a bit surprising that our calculated results are in excellent agreement with the experimental counterpart. In particular, our results directly show that the first two peaks close to the main line originate respectively from the ionizations of atoms C_2 (and C_2') and C_1 in Fig. 1(a) as well as their symmetric equivalent atoms on another $C_{59}N$ moiety, which confirms the conclusions in Ref. 14. One may notice however that the calculated spectrum is in general weaker than the experimental one after 4 eV. The neglect of the configuration interaction in the ECH-KS method will lose some details in the XPS shake satellites, which may account for the disagreement between the experimental and theoretical results. However, from our previous experience in the studies of the XPS shake-up satellites of fullerene C_{60} and single-walled carbon nanotubes,[29] the stronger intensities around 4–7 eV in the experiment may be due to the inelastic scattering of the photoelectrons between

TABLE II. Assignments of the nitrogen *K*-edge XPS shake-up satellites of the $C_{59}N$ family members.

	A	B
$C_{59}N$	HOMO → LUMO + 2 (α)	HOMO − 5 → LUMO + 2 (α)
$(C_{59}N)^+$	HOMO − 4 → LUMO	HOMO − 13 → LUMO
$C_{59}HN$	HOMO → LUMO + 2	HOMO → LUMO + 6
		HOMO − 5 → LUMO + 2
$(C_{59}N)_2$	HOMO → LUMO + 9	HOMO − 6 → LUMO + 8
	HOMO − 5 → LUMO + 2	HOMO − 18 → LUMO + 2
$C_{59}N$–C_{60}	HOMO → LUMO + 7 (α)	HOMO − 6 → LUMO + 9 (α)
	HOMO − 6 → LUMO + 2 (α)	HOMO − 19 → LUMO + 2 (α)
	HOMO − 4 → LUMO + 2 (β)	HOMO − 5 → LUMO + 9 (β)
	HOMO − 5 → LUMO + 2 (β)	HOMO − 18 → LUMO + 3 (β)
	HOMO − 5 → LUMO + 3 (β)	

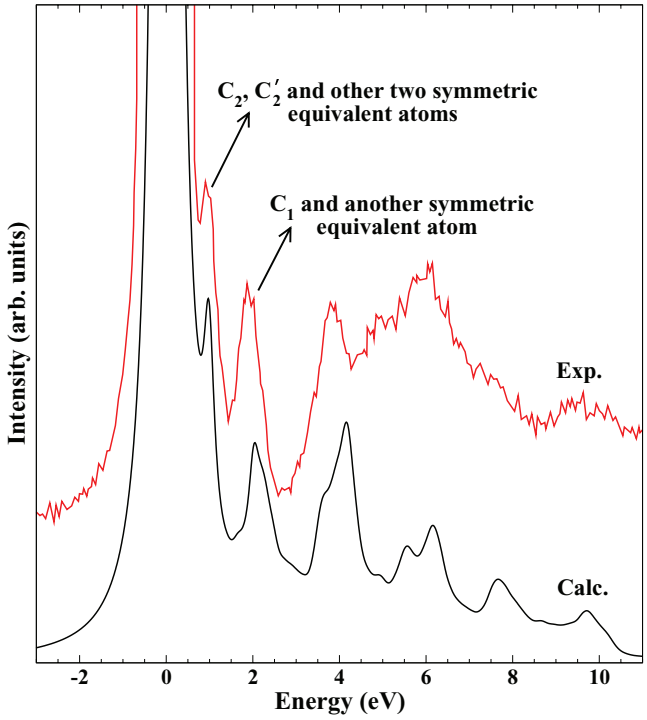

FIG. 9. Calculated XPS shake-up satellites of $(C_{59}N)_2$ molecule at the carbon *K*-edge and the experimental results taken from Ref. 14. The calculated results have been shifted so that the observable main line from calculations is at 0 eV to be able to compare with the experimental counterpart.

the $(C_{59}N)_2$ molecules during measurement, which could artificially increase the intensities of the shake-up spectrum in this energy range.

IV. CONCLUSIONS

We have in the present work demonstrated the usefulness of core-hole excitation spectra—NEXAFS, XES, and XPS shake-up satellites—in the study of the azafullerene $C_{59}N$ and its derivatives $(C_{59}N)^+$, $C_{59}HN$, $(C_{59}N)_2$ and the newly found heterodimer $C_{59}N$–C_{60}.[17] These spectra in general provide us detailed information of the unoccupied and occupied molecular orbitals of interested systems. For instance, the peak A′ around 284.5 eV in the carbon *K*-edge NEXAFS spectrum of the heterodimer $C_{59}N$–C_{60} (see Figs. 3 and 4) indicates the electron transfer from the $C_{59}N$ part to the C_{60} part in the heterodimer. Therefore, even as a weakly bonded molecule, the $C_{59}N$–C_{60} molecule does not show much similarities to its parent fullerene cages $C_{59}N$ and C_{60} in the electronic structures and different core-hole excitation spectra.

To distinguish the azafullerene $C_{59}N$ and its different derivatives, the nitrogen *K*-edge NEXAFS, XES, and XPS shake-up satellites spectra in general can be used. In particular with the help from theoretical simulations, we can gain in-depth understanding of the individual peaks in the experimental spectra and their relationships with the electronic and geometric structures of the investigated molecules.

The good agreement between our simulated results and available experimental data validates the use of the full core-hole potential and ΔKohn-Sham methods to predict the NEXAFS spectra and the use of our developed ECH-KS approach[29] for the simulations of the XPS shake-up satellites of the azafullerene $C_{59}N$ and its different derivatives. In particular, the latter will be served as an efficient and accurate computational approach for the studies of XPS shake-up satellites in large-scale molecules.

ACKNOWLEDGMENTS

We acknowledge the support from the Construction Project for Guizhou Provincial Key Laboratories (ZJ[2011]4007). B.G. thanks the support from the Research Council of Norway through a Centre of Excellence grant (Grant No. 179568/V30) and support from the Norwegian Supercomputing Program (NOTUR) through a grant of computer time (Grant No. NN4654K). M.S.D. acknowledges the support by the National Natural Science Foundation of China (No. 21203037), the Natural Science Foundation of Guizhou Province (No. QKH-J[2010]2144, J[2011]2097), and the Excellent Youth Scientific and Technological Talents of Guizhou Province (No. QKH-RZ[2013]01).

[1] J. C. Hummelen, C. Bellavia-Lund, and F. Wudl, Top. Curr. Chem. **199**, 93 (1999).
[2] U. Reuther and A. Hirsch, Carbon **38**, 1539 (2000).
[3] J. C. Hummelen, B. Knight, J. Pavlovich, R. González, and F. Wudl, Science **269**, 1554 (1995).
[4] B. Nuber and A. Hirsch, Chem. Commun. **12**, 1421 (1996).
[5] O. Vostrowsky and A. Hirsch, Chem. Rev. **106**, 5191 (2006).
[6] T. Pichler, M. Knupfer, R. Friedlein, S. Haffner, B. Umlauf, M. Golden, O. Knauff, H.-D. Bauer, J. Fink, M. Keshavarz-K, C. Bellavia-Lund, A. Sastre, J. Hummelen, and F. Wudl, Synth. Met. **86**, 2313 (1997).
[7] J. Auerhammer, T. Kim, M. Knupfer, M. Golden, J. Fink, N. Tagmatarchis, and K. Prassides, Solid State Commun. **117**, 697 (2001).
[8] T. Pichler, M. Knupfer, M. S. Golden, S. Haffner, R. Friedlein, J. Fink, W. Andreoni, A. Curioni, M. Keshavarz-K, C. Bellavia-Lund, A. Sastre, J.-C. Hummelen, and F. Wudl, Phys. Rev. Lett. **78**, 4249 (1997).
[9] H. Kuzmany, W. Plank, J. Winter, O. Dubay, N. Tagmatarchis, and K. Prassides, Phys. Rev. B **60**, 1005 (1999).
[10] F. Simon, D. Arčon, N. Tagmatarchis, S. Garaj, L. Forro, and K. Prassides, J. Phys. Chem. A **103**, 6969 (1999).
[11] M. Bühl, A. Curioni, and W. Andreoni, Chem. Phys. Lett. **274**, 231 (1997).
[12] S. Haffner, T. Pichler, M. Knupfer, B. Umlauf, R. Friedlein, M. S. Golden, J. Fink, M. Keshavarz-K., C. Bellavia-Lund, A. Sastre, J. C. Hummelen, and F. Wudl, Eur. Phys. J. B **1**, 11 (1998).
[13] K. Schulte, L. Wang, P. J. Moriarty, K. Prassides, and N. Tagmatarchis, J. Chem. Phys. **126**, 184707 (2007).
[14] K. Schulte, L. Wang, K. Prassides, N. Tagmatarchis, and P. J. Moriarty, J. Phys.: Conf. Ser. **100**, 072024 (2008).
[15] W. Andreoni, A. Curioni, K. Holczer, K. Prassides, M. Keshavarz-K., J.-C. Hummelen, and F. Wudl, J. Am. Chem. Soc. **118**, 11335 (1996).
[16] F. Fülöp, A. Rockenbauer, F. Simon, S. Pekker, L. Korecz, S. Garaj, and A. Jánossy, Chem. Phys. Lett. **334**, 233 (2001).
[17] A. Rockenbauer, G. Csányi, F. Fülöp, S. Garaj, L. Korecz, R. Lukács, F. Simon, L. Forró, S. Pekker, and A. Jánossy, Phys. Rev. Lett. **94**, 066603 (2005).
[18] J. Zhao, C. Zeng, X. Cheng, K. Wang, G. Wang, J. Yang, J. G. Hou, and Q. Zhu, Phys. Rev. Lett. **95**, 045502 (2005).
[19] G. Csányi and T. Arias, Chem. Phys. Lett. **360**, 552 (2002).
[20] J. Schrier and K. B. Whaley, J. Phys. Chem. A **110**, 5386 (2006).
[21] M. Keshavarz-K, R. González, R. G. Hicks, G. Srdanov, V. I. Srdanov, T. G. Collins, J. C. Hummelen, C. Bellavia-Lund, J. Pavlovich, F. Wudl, and K. Holczer, Nature (London) **383**, 147 (1996).
[22] F. Hauke and A. Hirsch, Tetrahedron **57**, 3697 (2001).
[23] M. Butcher, F. Jones, B. Cotier, M. Taylor, P. Moriarty, P. Beton, K. Prassides, N. Tagmatarchis, C. Comicioli, C. Ottaviani, and C. Crotti, Mater. Sci. Eng., B **74**, 202 (2000).

[24]M. Nyberg, Y. Luo, L. Triguero, L. G. M. Pettersson, and H. Ågren, Phys. Rev. B **60**, 7956 (1999).
[25]A. Bassan, M. Nyberg, and Y. Luo, Phys. Rev. B **65**, 165402 (2002).
[26]B. Gao, L. Liu, C. Wang, Z. Wu, and Y. Luo, J. Chem. Phys. **127**, 164314 (2007).
[27]B. Brena, S. Carniato, and Y. Luo, J. Chem. Phys. **122**, 184316 (2005).
[28]B. Brena, Y. Luo, M. Nyberg, S. Carniato, K. Nilson, Y. Alfredsson, J. Åhlund, N. Mårtensson, H. Siegbahn, and C. Puglia, Phys. Rev. B **70**, 195214 (2004).
[29]B. Gao, Z. Wu, and Y. Luo, J. Chem. Phys. **128**, 234704 (2008).
[30]M. J. Frisch, G. W. Trucks, H. B. Schlegel, *et al.*, Gaussian 09, Revision C.01 Gaussian, Inc., Wallingford, CT, 2009.
[31]B. Gao, "First principles studies of carbon based molecular materials," Ph.D. thesis (Royal Institute of Technology, 2008).
[32]W. Hua, B. Gao, and Y. Luo, Prog. Chem. **24**, 964 (2012).
[33]U. von Barth and G. Grossman, Solid State Commun. **32**, 645 (1979).
[34]T. Privalov, F. Gel'mukhanov, and H. Ågren, Phys. Rev. B **64**, 165115 (2001).
[35]T. Privalov, F. Gel'mukhanov, and H. Ågren, Phys. Rev. B **64**, 165116 (2001).
[36]L. Triguero, L. G. M. Pettersson, and H. Ågren, Phys. Rev. B **58**, 8097 (1998).
[37]B. Brena and Y. Luo, J. Chem. Phys. **119**, 7139 (2003).
[38]J. Qi, W. Hua, and B. Gao, Chem. Phys. Lett. **539–540**, 222 (2012).
[39]W. Kutzelnigg, U. Fleischer, and M. Schindler, *NMR Basic Principles and Progress* (Springer Verlag, Heidelberg, 1990), Vol. **23**, p. 165.
[40]A. D. Becke, Phys. Rev. A **38**, 3098 (1988).
[41]J. P. Perdew, Phys. Rev. B **33**, 8822 (1986).
[42]K. Hermann, L. Pettersson, M. Casida, C. Daul, A. Goursot, A. Koester, E. Proynov, A. St-Amant, and D. Salahub, StoBe-deMon, version 3.0 (2007).
[43]G. Vall-llosera, B. Gao, A. Kivimäki, M. Coreno, J. Álvarez Ruiz, M. de Simone, H. Ågren, and E. Rachlew, J. Chem. Phys. **128**, 044316 (2008).
[44]B. Gao, J. Jiang, K. Liu, and Y. Luo, BioNano-LEGO, Version 2.0, Royal Institute of Technology, Sweden (2008).
[45]R. L. Martin and D. A. Shirley, J. Chem. Phys. **64**, 3685 (1976).
[46]T. Åberg, Phys. Rev. **156**, 35 (1967).
[47]R. Manne and T. Åberg, Chem. Phys. Lett. **7**, 282 (1970).
[48]S. Lunell, C. Enkvist, M. Agback, S. Svensson, and P. A. Brühwiler, Int. J. Quantum Chem. **52**, 135 (1994).
[49]S. Lunell, M. P. Keane, and S. Svensson, J. Chem. Phys. **90**, 4341 (1989).
[50]B. Sjögren, J. Chem. Phys. **96**, 8338 (1992).
[51]B. Brena and Y. Luo, Radiat. Phys. Chem. **75**, 1578 (2006).
[52]A. Henderson, *ParaView Guide: A Parallel Visualization Application* (Kitware Inc., New York, 2007).
[53]D. V. Konarev and R. N. Lyubovskaya, Russ. Chem. Rev. **68**, 19 (1999).
[54]B. Gao, Z. Wu, H. Ågren, and Y. Luo, J. Chem. Phys. **131**, 034704 (2009).